ACS OMEGA

http://pubs.acs.org/journal/acsodf

Article

Evaluating Allosteric Perturbations in Cannabinoid Receptor 1 by *In Silico* Single-Point Mutation

Oscar Díaz, Pedro Renault,* and Jesús Giraldo*

Cite This: *ACS Omega* 2022, 7, 37873−37884

Read Online

ACCESS | Metrics & More | Article Recommendations | Supporting Information

ABSTRACT: Cannabinoid receptor 1 (CB1) is a promising drug target involved in many physiological processes. Using atomistic molecular dynamics (MD) simulations, we examined the structural effect of F237L mutation on CB1, a mutation that has qualitatively similar effects to allosteric ligand ORG27569 binding. This mutation showed a global effect on CB1 conformations. Among the observed effects, TM6 outward movement and the conformational change of the NPxxY motif upon receptor activation by CB1 agonist CP55940 were hindered compared to *wt* CB1. Within the orthosteric binding site, CP55940 interactions with CB1 were altered. Our results revealed that allosteric perturbations introduced by the mutation had a global impact on receptor conformations, suggesting that the mutation site is a key region for allosteric modulation in CB1.

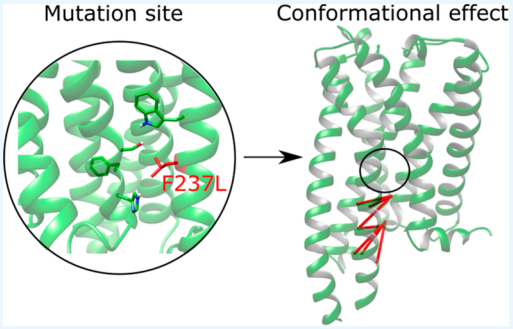

INTRODUCTION

Cannabinoid receptor 1 (CB1) is one of the key components of the endocannabinoid system. CB1 belongs to the class A G protein-coupled receptor (GPCR) family, is one of the most abundantly expressed GPCRs in the brain, and is involved in the modulation of pain, behavior, memory, and cognition.[1,2] CB1 is one of the targets of Δ^9-tetrahydrocannabinol (THC), the major psychoactive component of the cannabis plant, which has been consumed over millennia for recreational and medical uses.[3] Thus, the pharmacological properties of drugs that bind to cannabinoid receptors (cannabinoids) have been extensively studied over the years, including their endogenous ligands (endocannabinoids), cannabinoids present in the cannabis plant such as THC, and synthetic cannabinoids.[2,4,5] Although synthetic THC and a synthetic analogue (nabilone) are approved for medical use in the United States and in several countries in the EU (see ref 6 for a review on approved medications in the EU countries), the development of synthetic cannabinoid drugs with clinical use has been difficult. Specifically, inverse agonist SR141716A (rimonabant) was withdrawn from the market due to its apparent association to depression and suicidal ideation.[5,7] Given the difficulty of developing drugs that target the CB1 orthosteric site, allosteric modulation has emerged as an interesting approach to regulate the effects exhibited by orthosteric ligands. Importantly, allosteric compounds have known advantages over orthosteric ligands, such as a ceiling effect (in contrast to the effect of competition with a different orthosteric ligand, which can indefinitely shift the response of the endogenous ligand in a dose-dependent manner, the functional effects of allosteric modulators are "saturable", with a ceiling driven by the cooperativity between ligands and thus may offer an advantage to avoid overdose) and greater GPCR subtype-selectivity.[8,9] Allosteric modulators can increase (positive allosteric modulators, PAMs) and decrease (negative allosteric modulators, NAMs) the functional response exerted by orthosteric ligands or the receptor itself[10] or provide bias toward a particular signaling pathway (biased allosteric modulators, BAMs).[11] The first allosteric modulator targeting CB1 (ORG27569) was discovered in 2005,[12] but many others have since been discovered.[13−16]

Currently, a crystal structure of CB1 with bound ligands CP55940 (orthosteric agonist) and ORG27569 (allosteric modulator) is available.[17] In this structure, the orthosteric binding site is adapted for CP55940 binding but the intracellular region is in an inactive-like conformation. This structure confirmed the known pharmacologic behavior of ORG27569: positive allosterism for binding and negative allosterism for function,[12] known as a PAM-antagonist.[18] Moreover, this crystal structure shows ORG27569 bound to the intracellular region of transmembrane helix (TM) 2 and TM4, in an extrahelical cavity in contact with the membrane.[17] This binding site overlaps with a cholesterol binding site in CB1 as shown by agonist-bound crystal structures of CB1.[19] Consequently, ORG27569 competes with cholesterol binding, as described previously in rat brain membranes.[20] Interestingly,

Received: August 4, 2022
Accepted: September 28, 2022
Published: October 14, 2022

https://doi.org/10.1021/acsomega.2c04980
ACS Omega 2022, 7, 37873−37884

cholesterol enrichment reduces CP55940 binding,[21] while cholesterol depletion decreases inverse agonist binding,[20] suggesting cholesterol behaves as a NAM. This indicates this cavity contains key residues that affect orthosteric ligand binding and receptor activation, despite not being part of the orthosteric binding site or the G protein binding site.

Recently, parallel tempering metadynamics simulations indicated that a shift in F155$^{2.42}$ (Ballesteros-Weinstein numbering scheme included as a superscript[22]), a residue located in this cavity, is critical for receptor activation, and this rearrangement displayed a higher energy barrier than TM6 outward movement.[23] This shift of F155$^{2.42}$ can be observed by comparing inactive and active G protein-bound crystal structures of CB1, where F155$^{2.42}$ points toward the overlapping binding site of ORG27569 and cholesterol in the active receptor.[24−26] Another residue located at the overlapping binding pocket is F237$^{4.46}$. Mutation of this residue to leucine has been shown to increase CP55940 affinity and reduce inverse agonist SR141716A affinity.[17] As for its functional effect, it has been proposed that F237$^{4.46}$ has a role in the activation process.[17] In active crystal structures of CB1 with cocrystallized G protein,[25,26] F237$^{4.46}$ is displaced toward the extrahelical site and away from TM2 and TM3 (overlapping with the binding pose of ORG27569) and its space is replaced by F155$^{2.42}$, which shifts toward TM4 (Figure 1). This shift of

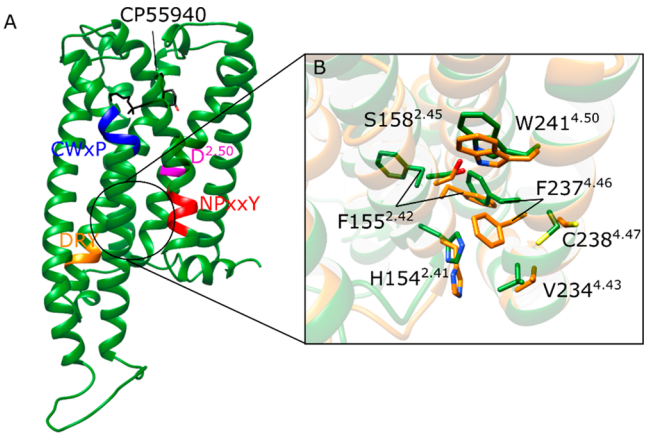

Figure 1. (A) View of the inactive *wt* CB1 model with bound CP55940 and with conserved sequence motifs in class A GPCRs highlighted. (B) Close up view of the extrahelical cavity in the inactive state (green, from PDB ID 5U09) and active state (orange, from PDB ID 6KPG) containing ORG27569 and cholesterol contact residues.

F155$^{2.42}$ and F237$^{4.46}$ is not tied to intracellular conformational changes in TM6 and TM7, which can be observed in active-like agonist-bound crystal structures of CB1 without bound G protein,[19] since F155$^{2.42}$ and F237$^{4.46}$ are in an "inactive-like" state in these structures. Interestingly, a cholesterol molecule is bound to the extrahelical cavity in these active-like crystal structures. Overall, this indicates CB1 activation is sensitive to perturbations in this region, which may be introduced by allosteric ligand binding, residue mutation or membrane lipid composition. Furthermore, F237$^{4.46}$ is not part of well-known sequence motifs or activation microswitches in class A GPCRs despite its capability to modulate ligand binding.

In this study, we investigate structural and dynamical effects of the F237L mutation. This work follows a previous study on the molecular mechanism of agonist-mediated CB1 activation.[27] In that study, starting from an inactive crystal structure of CB1,[24] we performed unbiased, microsecond-length molecular dynamics (MD) simulations in the apo state and also bound to the agonist CP55940, and observed spontaneous transitions to active-like states. This model included the protonation of some selected residues shown to favor active-like conformations (see Methods section). Thus, it provides a reference for comparison with subsequent studies on CB1. Here, we perform additional MD simulations to explore the perturbations on CB1 introduced by F237L mutation, as a model for allosteric perturbation at the allosteric site observed in crystal structures,[17,19] and evaluate their effects on CP55940-mediated CB1 activation. To do this, we employ the same CB1 model as presented in Díaz et al.[27] so as to compare the F237L mutant to *wt* CB1.

MATERIALS AND METHODS

The *wt* CB1 model employed was previously used in Díaz et al.[27] Briefly, the model was built from starting coordinates of the inactive crystal structure of CB1[24] obtained from the Protein Data Bank (PDB 5U09). After removal of the cocrystallized fusion protein, T210A mutation was restored to *wt* and the missing regions of TM5, TM6, and ICL3 were modeled using MODELER v9.14.[28] Then, the receptor was energy minimized, and CP55940 was docked into the orthosteric binding site using AUTODOCK4.2.[29] After our simulations with this model in Díaz et al.,[27] an inactive structure of CB1 with cocrystallized CP55940 was published.[17] Nevertheless, to allow direct comparisons with these earlier simulations, we kept the same protocol here and used the model built with docking. In the present study, the F237L mutant CB1 was generated from this previous model by replacing F237$^{4.46}$ with the leucine rotamer with highest probability in CHIMERA 1.14[30] according to the Dunbrack library.[31] Then, models of F237L CB1 and *wt* CB1 were minimized in CHIMERA 1.14 performing 1000 steps of steepest descent and 100 conjugate gradient steps in the AMBER14SB force field.

Molecular dynamics (MD) simulations of *wt* CB1 analyzed in this study at apo and CP55940-bound conditions were previously published in Díaz et al.[27] In two replicas of these simulations, starting from the inactive state, *wt* CB1 achieved active-like conformations when bound to CP55940. Therefore, they provide a good point of comparison to evaluate CB1 activation. The same MD simulation approach was employed for F237L CB1. The C257^{ECL2}-C264^{ECL2} disulfide bridge was maintained, and charges for D163$^{2.50}$, D213$^{3.49}$, E323^{ICL3}, D324^{ICL3}, D333$^{6.25}$, and D338$^{6.30}$ were neutralized, while H302$^{5.66}$, H304$^{5.68}$, and H320^{ICL3} were protonated.[27] Compared to the expected residue protonation state at pH 7, this alternative protonation state was shown to promote activation of CB1[27] and other class A GPCRs.[32−34] Systems were embedded in 80 × 80 Å 1-palmitoyl-2-oleoyl-*sn*-glycero-3-phosphocoline (POPC) homogeneous membranes, and the system charge was neutralized at 0.15 M concentration of KCl. Simulations were performed using ACEMD software[35] in the CHARMM36 force field[36] at 300 K and 1 atm, while CP55940 was parametrized in the CHARMM GenFF[37] using ParamChem.[38] Equilibration consisted in 8 ns of simulation time progressively releasing restraints on protein and ligand heavy atoms followed by 20 ns of simulation without restraints, and then each production run consisted of 2 μs of simulation time. MD simulation input files are provided in Supporting Information. Three replicas were performed for each

https://doi.org/10.1021/acsomega.2c04980
ACS Omega 2022, 7, 37873−37884

simulation condition (apo and agonist-bound *wt* CB1; apo and agonist-bound mutant), adding up to a total of 24 μs of simulation time analyzed in this study.

Trajectories were analyzed by examining MD-generated snapshots at an interval of 4 ns of simulation time. These MD-generated conformations were visually inspected and distances between Cα atoms of R214$^{3.50}$-D338$^{6.30}$ (residues implicated in the formation of the ionic lock), side chain hydroxyl atoms of Y294$^{5.58}$-Y397$^{7.53}$ and the χ_1 dihedral angles of W356$^{6.48}$, F200$^{3.36}$, F155$^{2.42}$, and F237$^{4.46}$ were measured using VMD 1.9.3.[39] Distances between aromatic moieties of F155$^{2.42}$, F237$^{4.46}$, and W241$^{4.50}$ were measured from the center of mass of the heavy atoms of aromatic rings in VMD, and the presence of aromatic interactions was considered when this distance was within a 7.0 Å distance cutoff.

Protein root-mean square deviation (RMSD) was also measured in VMD based on C_α atoms of transmembrane helices and taking the initial structure as reference. Ligand RMSD was based on its heavy atoms and measured against the initial docking pose. The initial CP55940 docking pose was compared to crystal structures with cocrystallized CP55940 (PDB 6KQI[17] and 7WV9[23]), and contact residues were defined as those within 4 Å of CP55940 heavy atoms.

Principal component analysis (PCA) was performed with GROMACS.[40] To do this, all replicas of agonist-bound *wt* and agonist-bound mutant CB1 were concatenated and aligned to the Cα atoms of the initial model. The N-terminal and the highly flexible ICL3 were excluded and not considered in the analysis. Therefore, only residues from A118$^{1.34}$ to R307$^{5.71}$ and from A335$^{6.27}$ to F412^{H8} were included in PC calculations. Then, we built and diagonalized the covariance matrix corresponding to this concatenated and aligned trajectory. The elements of this matrix were $C_{ij} = \langle(\mathbf{r}_i - \langle \mathbf{r}_i \rangle)(\mathbf{r}_j - \langle \mathbf{r}_j \rangle)\rangle$ where i and j denote the Cartesian coordinates of the Cα atoms of the receptor. The vector $\mathbf{r}_i$ indicates the instantaneous value of coordinate i and $\langle \mathbf{r}_i \rangle$ is the average value of this coordinate in the ensemble of conformations. Each individual trajectory was then projected on the space of the first two principal components.

The statistical analysis of pairwise residue distances was performed using the Ensemble Difference Distance Matrix, implemented in the Bio3D package in R.[41] Residue distances were compared between two groups, based on the results of PCA: (i) replicas 2 and 3 of agonist-bound *wt* CB1 and (ii) all replicas of agonist-bound F237L CB1. The distance between two residues was defined as the closest distance between any heavy atoms in the residues (side chains included). Residue pairs whose distances were greater than 10 Å across all frames of all trajectories were excluded from the analysis. In the same manner as PCA, the N-terminal and the ICL3 were also excluded (only residues from A118$^{1.34}$ to R307$^{5.71}$ and from A335$^{6.27}$ to F412^{H8} were considered). Matrices of the average distances between residues were built for the two groups and a difference distance matrix was obtained by subtracting the matrix of the mutant from that of the *wt* receptor; however, only statistically significant differences greater than 1 Å were retained. Statistical significance was determined by a two-sample Wilcoxon test, with p-value lower than 0.005. To identify close contacts that were present in one group but not in other, we selected a subset of the significant differences in which the average residue distance was lower than a 4 Å cutoff in one group and greater than this cutoff in the other.

In order to characterize differences in the interaction frequencies between agonist and contacting residues for both *wt* and F237L CB1, first the distance between the closest heavy atoms of CP55940 and the receptor for each trajectory frame was measured using *gmx pairdist* in GROMACS.[40] Then, contact frequencies for each residue were calculated considering that a contact is present if the distance is <4 Å. Finally, the frequencies for CP55940-F237L CB1 contacts were subtracted from the frequencies for *wt* CB1 for each respective residue to generate a frequency difference. As a second approach, ΔG_{bind} was estimated using gmx_MMPBSA,[42] including an implicit membrane with thickness determined by CHARMM-GUI initial setup. Solvent, membrane, and internal dielectric constants used were 80, 7, and 2, respectively. Residues within 4 Å of the starting CP55940 binding position and residues that showed average difference in contact frequency over 0.1 were considered for decomposition analysis. Average differences in free energy decomposition were evaluated by a two-sample, two-tailed Student's t test, with equal or unequal variances as assessed by an F-test.

Water occupancy was defined as the percentage of frames in which a given protein residue established a contact (distance within 4 Å) with a water molecule. Distances between protein and water were measured with the tool *gmx pairdist* in GROMACS.[40]

RESULTS

Overall, MD trajectories were stable, as indicated by the RMSD curves in Figure S1. Higher values were observed for two of the replicas of agonist-bound *wt* receptor (Figure S1A), and this is consistent with the conformational changes seen in these trajectories, where CB1 achieved active-like conformations,[27] characterized by a movement of TM6 (Figure S1E). In comparison to *wt* systems, the RMSD was higher in trajectories of the mutant, and this can be explained by the relaxation that followed the perturbation introduced by the mutation (Figure S1B, D, F). Plots of the root mean square fluctuation (RMSF) also point to a consistent pattern of CB1 fluctuations in all trajectories (Figure S2).

The RMSD of the agonist CP55940 was relatively high (Figure S3B, C), and probably reflected inaccuracies introduced by docking. As shown in Figure S3A, the docking pose differs from the crystal structure (PDB 6KQI) mainly in the position of the C ring and the orientation of its OH groups (Figure S4A). As a result, native contacts between the ligand and TM2 are missing from the docking pose. Overall, from 19 protein−ligand contacts present in the crystal structure, 12 were found in docking (63%). In addition, contacts with I267^{ECL2} and L276$^{5.40}$ were frequently formed during the simulations, raising the percentage of native contacts retained from the crystal structure to 74%. More details about the frequency of CB1-CP55940 contacts in the simulations can be found in Table S1. Nevertheless, CP55940 remained in its binding site throughout the MD trajectories (Figure S3B, C), despite fluctuations observed mostly due to movement of its alkyl chain and, to a lesser extent, its C-ring (Figure S4). Moreover, as active-like conformations were generated in CP55940-bound CB1 but not in apo,[27] this indicates that our model captures native contacts that are likely important for receptor activation. Taken together, these observations suggest that, despite inaccuracies introduced by docking, and considering that MD simulations of F237L CB1 started from

https://doi.org/10.1021/acsomega.2c04980
ACS Omega 2022, 7, 37873−37884

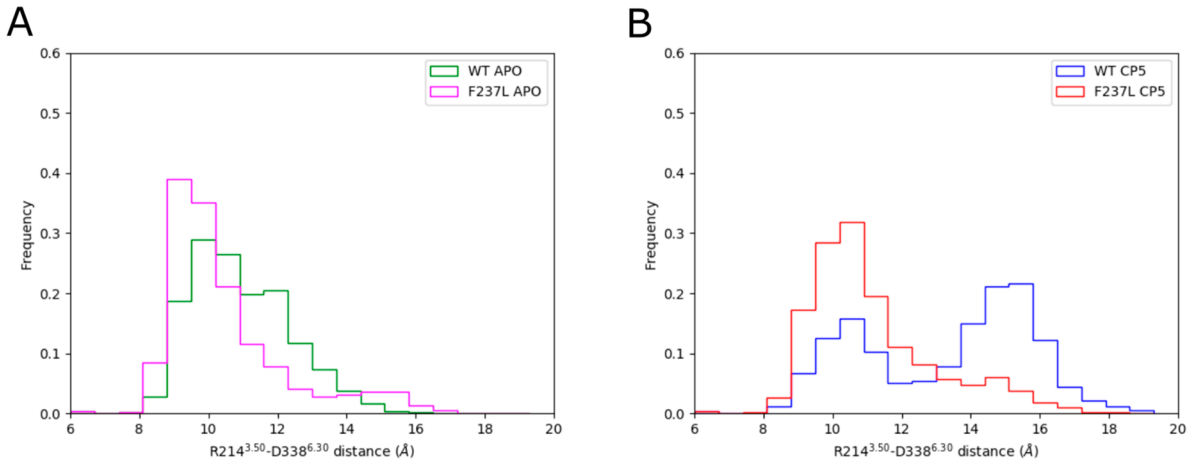

Figure 2. Distribution of the R214$^{3.50}$-D338$^{6.30}$ distance in MD simulations of (A) apo CB1 and (B) CP55940-bound CB1. Data from all replicas; MD snapshots were collected at a 4 ns time interval in each one of them. Histograms for *wt* CB1 were calculated from MD simulations published in Díaz et al. 2019.

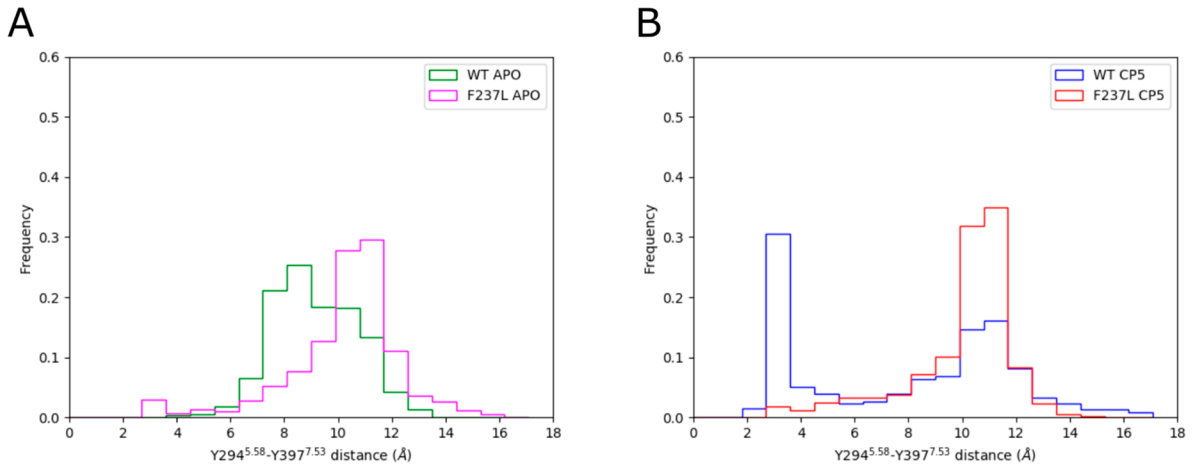

Figure 3. Distribution of the distance between side chain oxygen atoms of Y294$^{5.58}$ and Y397$^{7.53}$ in MD simulations of (A) apo CB1 and (B) CP55940-bound CB1. Data from all replicas; MD snapshots were collected at a 4 ns time interval in each one of them. Histograms for *wt* CB1 were calculated from MD simulations published in Díaz et al.[27]

the same initial model, it was still possible to discern the effect of the mutation on collective motions of the receptor.

F237L Mutation Hindered Outward Movement of TM6. The hallmark of class A GPCR activation is the breakage of the salt-bridge formed by residues 3.50 and 6.30 (ionic lock) and consequent outward movement of TM6 away from TM3,[43] which can be observed by comparing inactive and active CB1 crystal structures.[19,23−26,44] In our MD simulations of apo CB1, TM6 remained in inactive-like conformations both in *wt* and F237L CB1, as shown by the distance between residues R214$^{3.50}$-D338$^{6.30}$ (Figure 2A), which is expected because CB1 was in the inactive conformation at the start of MD simulations. In CP55940-bound *wt* CB1 MD simulations, TM6 moved outward, reaching active-like states in two of the three replicas performed.[27] Thus, two subpopulations of TM6 conformation can be observed: an inactive-like conformation that is represented by a closer R214$^{3.50}$-D338$^{6.30}$, and an active-like conformation represented by a larger TM3-TM6 distance, indicating a broken ionic lock (blue curve in Figure 2B). On the contrary, this did not occur in F237L mutant CB1 (red curve in Figure 2B) even when CP55940 was bound to the receptor. Here, TM6 remained mostly in an inactive-like conformation, similar to the observations in apo conditions. This indicates the outward movement of TM6 upon receptor activation by CP55940 was hindered by F237L mutation, and this is consistent with a role of F237$^{4.46}$ on receptor activation.[17,25]

F237L Mutation Blocked Y397$^{7.53}$ Conformational Change. At the receptor level, the binding of a signaling protein is the final consequence of receptor activation. In this regard, the NPxxY motif has been linked to G protein binding, as Y397$^{7.53}$ shifts toward Y294$^{5.58}$ in active receptor conformations to facilitate G protein binding and blocking TM6 inactivation.[25,43] In MD simulations of apo CB1, Y397$^{7.53}$ remained in an inactive-like conformation overall, as shown by the distance between Y397$^{7.53}$ and Y294$^{5.58}$ (Figure 3A), regardless of F237L mutation. In contrast, a new population was observed in *wt* CB1 bound to CP55940 centered at ∼3 Å, indicating the presence of active-like conformations[27] (blue curve in Figure 3B). However, this subpopulation was not clearly represented in CP55940-bound F237L CB1 (red curve in Figure 3B), where Y397$^{7.53}$ remained in inactive-like conformations such as in apo CB1. This suggests that F237L mutation blocks the conformational change in Y397$^{7.53}$ observed in active crystal structures of CB1.[25,26] Together with the hindrance of TM6 movement, our results indicate that

https://doi.org/10.1021/acsomega.2c04980
ACS Omega 2022, 7, 37873−37884

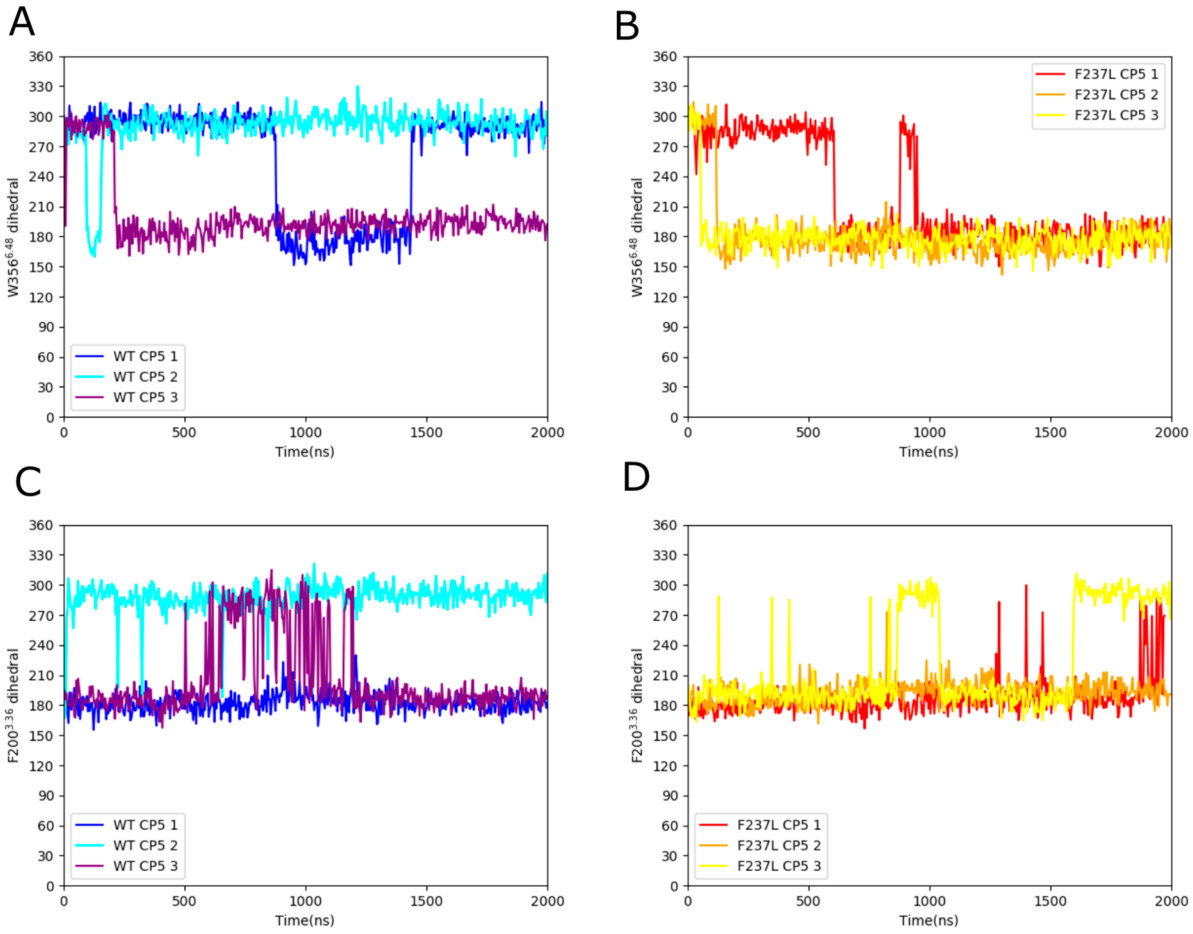

Figure 4. χ_1 dihedral angles of (A, B) W356$^{6.48}$ and (C, D) F200$^{3.36}$ along MD simulation time for three trajectories of (A, C) *wt* CB1* and (B, D) F237L CB1. *Data from MD simulations of *wt* CB1 taken from Díaz et al.[27]

F237L mutation interfered with receptor activation during the simulations.

W356$^{6.48}$/F200$^{3.36}$ Rotameric Switch Was Unaffected by F237L Mutation. The residue pair W356$^{6.48}$/F200$^{3.36}$ forms an additional microswitch for receptor activation in CB1, consisting of a double rotameric switch where W356$^{6.48}$ and F200$^{3.36}$ are rearranged upon receptor activation. This is accompanied by an upward movement of TM3.[27] This rearrangement has been proposed to be mediated by changes in the χ_1 dihedral angles of W356$^{6.48}$ and F200$^{3.36}$ that result in the breakage of aromatic stacking interactions between these two residues upon receptor activation.[25] McAllister et al., 2004 proposed W356$^{6.48}$ shifts its χ_1 dihedral angle from *gauche*(+) to *trans*, followed by a transition in the χ_1 dihedral angle of F200$^{3.36}$ from *trans* to *gauche*(+).[45] This was observed in MD simulations of *wt* CB1 as described in Díaz et al., 2019 (Figure 4A, C), although W356$^{6.48}$ conformation may return to *gauche*(+) after TM3 upward movement while the receptor is in an active-like conformation, as shown by active CB1 crystal structures.[25,26] In MD simulations of CP55940-bound F237L CB1 (Figure 4B, D), the χ_1 dihedral angle from W356$^{6.48}$ transitioned from *gauche*(+) to *trans* and χ_1 dihedral angle from F200$^{3.36}$ transitioned from *trans* to *gauche*(+), suggesting that the double rotameric switch was unaffected by F237L mutation.

Contacts between CP55940 and CB1 Were Affected by F237L Mutation. To evaluate the effect of F237L mutation on agonist binding, the frequencies of contact between CP55940 and CB1 were calculated for MD simulations of *wt* and mutant receptors. The difference in average frequencies between *wt* and mutant suggests there is a difference on how CP55940 interacts with CB1, with some interactions favored for *wt* and others for F237L (Figure 5). Moreover, interaction differences were consistent across simulation time (Figures S5 and S6).

Additionally, the affinity of CP55940 for *wt* and F237L CB1 was estimated using Molecular Mechanics Poisson−Boltzmann Surface Area (MMPBSA), decomposed for each residue within 4 Å of CP55940 starting conformation, in addition to residues identified by contact frequency difference analysis. Overall, the difference between global ΔG_{bind} for *wt* and F237L was not statistically significant as calculated by a two-sample Student's *t* test ($\Delta G_{bind}^{wt} = -12.22 \pm 0.52$ kcal/mol, $\Delta G_{bind}^{F237L} = -12.48 \pm 0.71$ kcal/mol (mean ± S.E.M.), $p = 0.583$, for $n = 3$ trajectories). From both contact frequency difference and MMPBSA decomposition, residues could be grouped according to whether their interaction with CP55940 was favored in *wt* or in F237L. According to frequency differences, residues favored by *wt* CB1 were most notably S123$^{1.39}$, F170$^{2.57}$, and M384$^{7.40}$, while residues favored by F237L CB1 were P269^{ECL2}, A380$^{7.36}$, C382$^{7.38}$, and C386$^{7.42}$. MMPBSA decomposition (Figure 5C) showed residues S123$^{1.39}$, F170$^{2.57}$, F200$^{3.36}$, L276$^{5.40}$, M384$^{7.40}$, and L387$^{7.43}$ were favored toward *wt* CB1, while residues L359$^{6.51}$, F379$^{7.35}$, A380$^{7.36}$, and C386$^{7.42}$ were favored toward F237L CB1. To a lesser extent, this analysis also indicated that interaction with residues

https://doi.org/10.1021/acsomega.2c04980
ACS Omega 2022, 7, 37873−37884

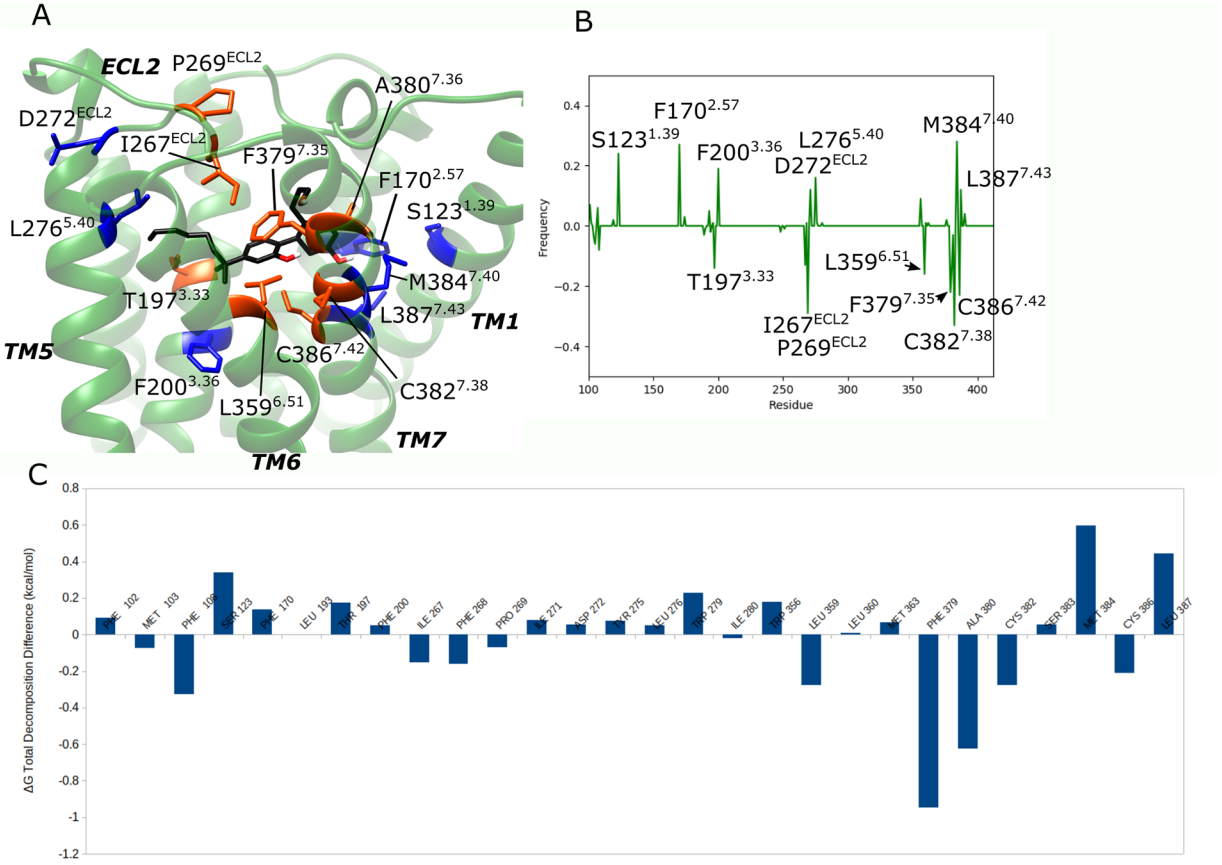

Figure 5. Contact analysis between CP55940 and CB1 in MD simulations. (A) Structural representation of contact frequencies favored by *wt* CB1 (blue) and by F237L CB1 (orange). (B) Difference between average contact frequencies per residue (residues are considered in contact if any of their heavy atoms is at <4 Å from the ligand). (C) Average difference in ΔG_{bind} decomposed for each residue interacting with CP55940, in *wt* and F237L CB1 (in kcal/mol). Positive values represent CP55940-CB1 interactions favored in *wt* CB1 (higher contact frequency or more negative ΔG), while negative values represent interactions favored in F237L CB1. MD trajectories of *wt* CB1 taken from Díaz et al.[27]

$I267^{ECL2}$, $F268^{ECL2}$, and $P269^{ECL2}$ was favored in F237L CB1. MMPBSA analysis is in qualitative agreement with the contact frequency analysis except for residue $T197^{3.33}$ (Figure 5B). However, none of the detected differences between *wt* and F237L CB1 was statistically significant (*p*-values summarized in Table S2).

Interestingly, many of the residues favored by F237L are close to the extracellular region of the receptor, including $I267^{ECL2}$, $F268^{ECL2}$, and $P269^{ECL2}$ which are in extracellular loop 2 (ECL2), and $F379^{7.35}$ in TM7, identified by both contact frequency and MMPBSA decomposition analyses. ECL2 is a critical region for CP55940 binding, as alanine substitutions at every position between $P269^{ECL2}$ and $I271^{ECL2}$ abolish CP55940 binding.[46] On the other hand, a mutation to A or W in $F170^{2.57}$, whose interaction with CP55940 was favored in *wt* CB1, does not alter the potency of CP55940.[44] Critical residues whose contacts with CP55940 were favored in *wt* CB1 include $M363^{6.55}$ and $S383^{7.39}$,[47,48] which were identified by MMPBSA decomposition analysis and not by contact frequency analysis, indicating that interaction of CP55940 with $M363^{6.55}$ and $S383^{7.39}$, while present in F237L CB1, were slightly stronger in *wt* CB1. Overall, our results suggest the contact pattern between CP55940 and F237L CB1 is altered in comparison with *wt* CB1 and interactions with residues located at extracellular regions of the receptor are favored in F237L CB1.

F237L Mutation Had a Global Effect on CB1. Distance distributions of residues $R214^{3.50}$-$D338^{6.30}$ and of residues $Y294^{5.58}$-$Y397^{7.53}$ (Figures 2 and 3, respectively) suggest that the effect of the mutation is more evident when CB1 is bound to the agonist. In order to obtain a general assessment of the impact of the mutation on the structure and dynamics of CB1 during the simulations of this condition, we performed a principal component analysis (PCA). We projected the trajectories of *wt* and mutant CB1 bound to CP55940 on a common vector space (obtained after concatenation of the trajectories; see details in the Methods section). These projections are shown in Figure 6A, where conformations explored in *wt* CB1 simulations are represented in blue and those in mutant CB1 simulations are in red. It is possible to see a substantial overlap between the region of the conformational space which was visited by replica 1 of the *wt* receptor (light blue) and the space collectively explored by the three replicas of the mutant receptor (in red). We note that replica 1 was precisely the only one in which *wt* CB1 did not achieve active-like conformations, and no consistent outward movement of TM6 was observed (see Figure S1). In contrast, the two other replicas of the *wt* system explored regions of the conformational space which were inaccessible to the mutant receptor, indicating that conformational changes were restricted by the mutation.

The features of such changes can be clarified by an inspection of the directions of collective motion that

https://doi.org/10.1021/acsomega.2c04980
ACS Omega 2022, 7, 37873−37884

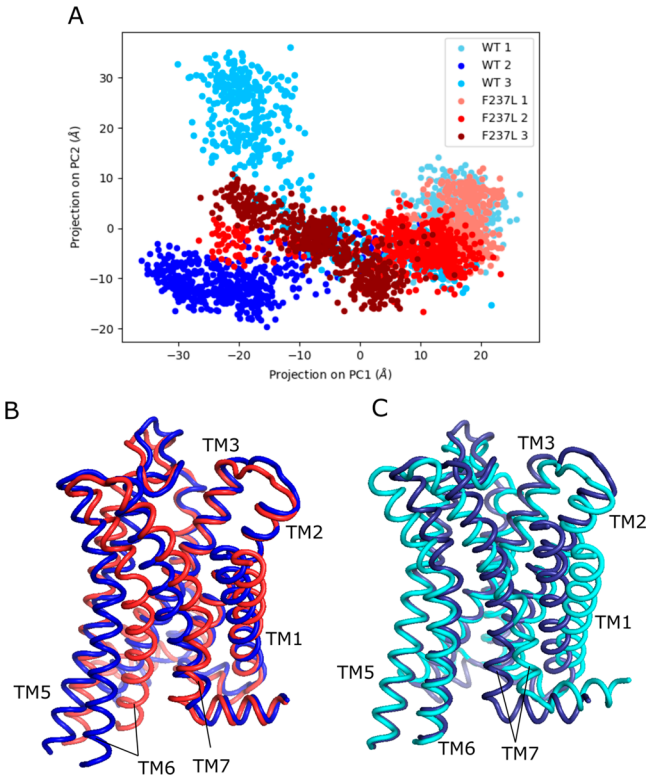

Figure 6. (A) Projection on the principal components PC1 and PC2 of the *wt* and F237L CB1 MD-generated conformations with bound CP55940. (B) Extreme conformations along the direction of PC1 (minimum value in blue, maximum value in red). A transition from the red to the blue conformation corresponds to a movement from positive to negative projections along the direction of PC1. (C) Extreme conformations along the direction of PC2 (minimum value in blue, maximum value in cyan). A transition from the blue to the cyan conformation corresponds to a movement from negative to positive projections along the direction of PC2.

correspond to PCs 1 and 2. Figure 6B shows that going from positive to negative values of the projection along PC1 (from right to left in the PC map in Figure 6A) corresponds to an outward motion of TM6. In the case of PC2, Figure 6C shows the motion from negative to positive values of the projection (from bottom to top in the PC map) corresponds to a bending of TM7 that contributes to open the intracellular cavity of the receptor (besides a collective rearrangement around the orthosteric site). Therefore, open and active-like conformations of CB1 are scarcely explored by the mutant. Taken together, these results indicate that the mutation had an impact on the dynamical behavior of CB1 and shifted the receptor population toward the inactive state.

As detailed in the Methods section, PCA was based on the Cα atoms of CB1, thus providing information on motions of the main chain. However, we also wanted to investigate how the mutation affected the side chains of the receptor. The residues analyzed in the previous sections are either microswitches of CB1 activation well established in the literature[25,26] or form the binding cavity of the orthosteric ligand, and thus were selected as a first indicator of the effect of F237L mutation. To characterize other residues that may be affected by F237L mutation, we calculated distance matrices of *wt* and mutant CB1, both in the presence of the agonist. PCA results allowed us to separate two groups for comparison in order to reduce noise and focus on differences between the two conditions: (i) replicas 2 and 3 of *wt* CB1 (where active-like conformations were observed); (ii) the three replicas of the mutant. We then determined statistically significant differences in average residue pairwise distances between these two groups. Residue pairs with distances always longer than 10 Å in all trajectories were excluded from the analysis. A list of the 1378 residue pairs whose variations in distance were significantly higher than 1 Å is available in the Supporting Information. Considering the magnitude of distance variations, the top 35 (variations in the range 4.6−6.7 Å) corresponded to distances that were larger in the *wt* receptor; interestingly, they involved residue pairs in TM6-TM2 and TM6-ICL2. It is necessary to descend to the 36th position in the ranking to find a residue pair with increased distance in the mutant, and it involved residues in TM7 and TM3. The 10 largest differences are listed in Table 1 and schematically depicted in Figure 7A,

Table 1. Top 10 Highest Differences in Average Residue Pairwise Distance between MD Simulations of *wt* (Replicas 2 and 3) and F237L CB1 (All Replicas) with Bound CP55940

residue 1	residue 2	avg. distance in *wt* (Å)	avg. distance in F237L (Å)	delta (Å)	*p* value
$P151^{2.38}$	$D338^{6.30}$	20.22	13.52	6.70	1.9×10^{-291}
$F155^{2.42}$	$L345^{6.37}$	11.98	6.00	5.98	1.9×10^{-254}
$S152^{2.45}$	$A342^{6.34}$	17.16	11.43	5.73	4.9×10^{-284}
$P151^{2.38}$	$L341^{6.33}$	15.88	10.19	5.69	2.9×10^{-275}
$F155^{2.42}$	$A342^{6.34}$	17.25	11.57	5.69	8.7×10^{-248}
$F155^{2.42}$	$V346^{6.38}$	16.15	10.45	5.69	9.6×10^{-244}
$P151^{2.38}$	$M337^{6.29}$	19.72	14.04	5.68	1.1×10^{-257}
$S152^{2.39}$	$L341^{6.33}$	12.68	7.04	5.64	7.5×10^{-277}
$S152^{2.39}$	$D338^{6.30}$	17.34	11.76	5.58	3.4×10^{-284}
$S152^{2.39}$	$I339^{6.31}$	19.59	14.06	5.53	3.7×10^{-276}

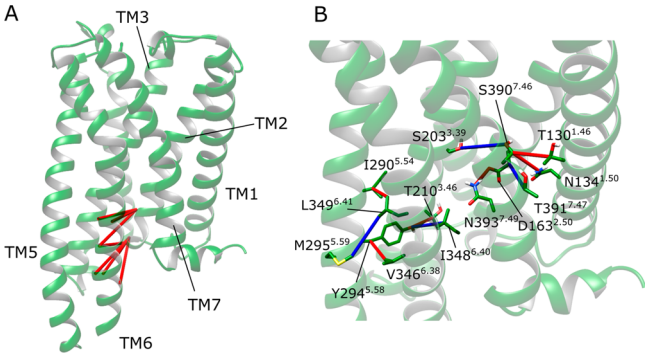

Figure 7. (A) Ten largest distance differences in MD simulations between *wt* CB1 (replicas 2 and 3) and F237L CB1 (all replicas) with bound CP55940. (B) Differences in contacts between *wt* CB1 (replicas 2 and 3) and F237L CB1 (all replicas) with bound CP55940. Contacts only present in *wt* CB1 are represented in blue and contacts only present in F237L are represented in red.

which shows that in *wt* CB1 there was a larger distance between TM6 and TM2 in comparison to the mutant. This increased distance was consistent across simulation time ($P151^{2.38}$-$D338^{6.30}$ distance shown in Figure S7). This is in agreement with our other results and indicates that an outward movement of TM6 was hindered by the mutation. It is also worth noting that the largest distance observed between TM7 and TM3 in the mutant is also consistent with the hypothesis

https://doi.org/10.1021/acsomega.2c04980
ACS Omega 2022, 7, 37873−37884

that the mutation suppresses collective motions that lead to activation, since the approach between these two helices is well described in the activation of class A GPCRs.[49]

Moreover, the hindrance of TM6 movement by the mutation was reflected by the higher frequency of water molecules in contact with residues A342$^{6.34}$ and I396$^{7.52}$ (close to the G protein binding cavity) in *wt* CB1 compared to F237L CB1 (Figure S8). The presence of these additional contacts with water molecules in this region suggests an entrance of water molecules as a consequence of the outward movement of TM6, and can be seen as an indicator of conformational change, which occurred in *wt* receptor and was hindered by the mutation.

In a complementary analysis, we also identified residues which formed close contacts (distance < 4 Å for at least 50% of the simulation time) in one group but not in the other (Table 2 and Figure 7B). In this category, we found residue pairs in

Table 2. Differences in Close Residue Contacts (Distance < 4 Å) between MD Simulations of *wt* (replicas 2 and 3) and F237L CB1 (All Replicas) with Bound CP55940

residue 1	residue 2	contact in *wt*	contact in F237L
S203$^{3.39}$	S390$^{7.46}$	yes	no
Y294$^{5.58}$	I348$^{6.40}$	yes	no
M295$^{5.59}$	L349$^{6.49}$	yes	no
D163$^{2.50}$	T391$^{7.47}$	yes	no
T130$^{1.46}$	S390$^{7.46}$	no	yes
N134$^{1.50}$	S390$^{7.46}$	no	yes
T210$^{3.46}$	Y294$^{5.58}$	no	yes
Y294$^{5.58}$	V346$^{6.38}$	no	yes
I290$^{5.54}$	L349$^{6.41}$	no	yes
D163$^{2.50}$	N393$^{7.49}$	no	yes

TM6-TM3 and TM6-TM5; and also pairs between TM7 and TM1, and between and TM2 and TM3. Residues D163$^{2.50}$, Y294$^{5.58}$, S390$^{7.46}$, and L349$^{6.41}$ were each one of them involved in more than one of these contacts which were switched on or off, suggesting an important role for these residues in the collective dynamics of CB1. Notably, many of these changing contacts, as well as the large amplitude distance variations, occurred far from the site of the mutation, involving several other helices and distinct regions of the receptor, pointing to the global structural and dynamical effect of the mutation.

F237L Substitution Disrupted Aromatic Interactions in the Mutation Site. F237L mutation consists of a substitution of an aromatic residue with an aliphatic one. In crystal structures of CB1, F237$^{4.46}$ is in the vicinity of two aromatic residues, F155$^{2.42}$ and W241$^{4.50}$; the latter is a highly conserved residue in class A GPCRs[50] which participates in allosteric modulator ORG27569 binding.[17] In one of the MD simulation replicas of *wt* CB1 bound to CP55940,[27] a conformational change of F155$^{2.42}$ and F237$^{4.46}$ was observed. In this MD trajectory, active-like conformations were observed[27] and F155$^{2.42}$ shifted toward TM4 generating an intermediate state in which F155$^{2.42}$ and F237$^{4.46}$ briefly formed aromatic tilted T-shape interactions (Figure S9), after which F237$^{4.46}$ shifted away from TM3. This configuration of F155$^{2.42}$ and F237$^{4.46}$ (Figure S9C) can be seen in active crystal structures of CB1 with cocrystallized G protein,[25,26] but not in active-like crystal structures without the G protein.[19] Aromatic interactions between F237$^{4.46}$ and W241$^{4.50}$ are favored in this "displaced" configuration of F237$^{4.46}$ (Figure S10). Thus, substitution of phenylalanine by leucine would disrupt such aromatic interactions between F237$^{4.46}$ and W241$^{4.50}$ characteristic of states coupled to the G protein. Presumably, this modulation might extend to ligand binding to this region because of the fact that ORG27569 and cholesterol bind to CB1 with an inactive-like conformation of F155$^{2.42}$ and F237$^{4.46}$.[17,19,23]

DISCUSSION AND CONCLUSIONS

In this study, we have interrogated the effect of the F237L mutation upon CB1 activation through molecular dynamics simulations. Here, we performed MD simulations of apo and CP55940-bound F237L CB1, starting from the inactive state of the receptor. We compared our observations with results from our previous work, in which we performed simulations of *wt* CB1.[27] In that work, we observed that the agonist-bound *wt* receptor achieved active-like conformations during the trajectories; in contrast, in the simulations of the mutant performed here CB1 remained inactive, even in the presence of the agonist. Notably, the mutation was associated to a suppression of a large amplitude outward movement of TM6 in the simulations.

In both of our studies—our previous work with *wt* CB1 and the present one with the mutant—systems were setup in the same way, and we followed the same simulation protocol. This included the insertion of the receptor in a very simple model membrane, composed of POPC. Though it has been shown that cholesterol can play an important role as an allosteric modulator of GPCRs,[51] and particularly of CB1,[20,21,52] it was not included in our simulations. This allowed us to make direct comparisons with our previous work and also to decouple the effect of the mutation from allosteric effects exerted by cholesterol. Moreover, F237$^{4.46}$ is located in a cholesterol binding site of CB1,[19] and an investigation of the impact of the mutation on cholesterol binding or the combined effects of cholesterol and the mutation were beyond the scope of this paper. However, it should be important to consider the behavior of the mutant receptor in the presence of cholesterol, and we believe this topic deserves attention in the future.

Crystal structures show that the conformation of F237$^{4.46}$ changes upon receptor activation, and this conformational change is accompanied by a rearrangement of F155$^{2.42}$ (see Figure 1B). In the inactive state,[24] F155$^{2.42}$ points toward the G protein binding cavity, interacting with residues L207$^{3.43}$, T210$^{3.46}$, L345$^{6.37}$, I348$^{6.40}$, and Y397$^{7.53}$ in other TMs. Upon activation,[25,26] F155$^{2.42}$ shifts and points toward the extracellular cavity and interacts with residues L209$^{3.45}$, D213$^{3.49}$, A233$^{4.42}$, and L237$^{4.46}$. This shift therefore leads to a loss of contacts between TM2 and TM6 which possibly facilitates the uncoupling between these two helices. The important role of F155$^{2.42}$ in CB1 activation has been recently highlighted by metadynamics simulations,[23] which indicated that the rearrangement of this residue (and, more generally, a rearrangement of TM2) is a critical step in CB1 activation. Importantly, these simulations revealed that the free energy barrier to the conformational change of F155$^{2.42}$ is much higher than the one associated to the outward movement of TM6. Our results are consistent with this picture, since the outward movement of TM6 was more frequently observed in our simulations than the reorientation of F155$^{2.42}$. Importantly, we should note that in our trajectories the F237L mutation hindered this relatively easier movement of TM6, suggesting

https://doi.org/10.1021/acsomega.2c04980
ACS Omega 2022, 7, 37873−37884

that the mutation contributes to heighten the energy barrier to the displacement of this helix.

The active-like states observed in our simulations were then frequently characterized by TM6 and F155$^{2.42}$ in active and inactive conformations, respectively (this also characterizes conformational states explored in the metadynamics simulations referred to above, in which TM6 could switch between inward and outward states while F155$^{2.42}$ remained in its inactive conformation). The existence of such distinct intermediate states is consistent with models of GPCR dynamics that propose the existence of multiple conformational states in dynamical equilibrium.[53] Other molecules—for instance, orthosteric or allosteric ligands, membrane lipids or intracellular proteins such as G proteins—would be able to shift this equilibrium and stabilize certain conformations, thus modulating the receptor function. For example, recent NMR experiments with CB1 in the presence of different ligands (including the agonist CP55940 and the allosteric modulator ORG27569) detected a variety of conformational states, leading the authors to propose a model for activation and allosteric modulation including not only inactive and active states but also preactive and active-like conformations; each one of them would be favored by the interaction with distinct partners.[54] In the particular case of the conformations of TM6 and F155$^{2.42}$, it is possible that the stabilization of both in the fully active conformation requires coupling to the G protein. Our results suggest that the F237L mutation renders G protein coupling less probable, because it shifts the dynamical equilibrium toward the inactive state of the receptor.

Structural differences between *wt* and mutant CB1 in the simulations were accompanied by modifications in the hydration of the receptor. In particular, *wt* CB1 exhibited a higher occupancy of water molecules in specific residues close to the G-protein binding site. The entrance of these water molecules was possibly facilitated by the outward movement of TM6, that opened the intracellular cavity. It constituted another indicator of conformational changes observed in *wt* CB1 and suppressed by the mutation. However, the observed differences in the pattern of hydration between *wt* and mutant CB1 are complex (Figure S8), and it remains to be verified if water molecules play an active part in triggering CB1 conformational changes, as suggested for the activation of other GPCRs.[55,56]

It seems logical to attribute the behavior of F237L mutation to the loss of aromatic interactions in the mutated receptor due to the substitution of an aromatic residue for an aliphatic one. It should be noted that, although our simulations indicated that stacking or T-shape aromatic interactions between F155$^{2.42}$ and F237$^{4.46}$ may form transiently in a dynamic context (Figure S9), aromatic interactions between these residues are not present in CB1 crystal structures. Moreover, in mutagenesis experiments the replacement of F155$^{2.42}$ by V, an aliphatic but smaller side chain, was shown to increase G_i signaling; in contrast, mutation to the aromatic but larger W had the opposite effect.[23] These results suggest the aromaticity of F155$^{2.42}$ might not be the determinant factor for its role in the activation process, and also the possibility that the size of the side chain at this location might be important.

On the other hand, W241$^{4.50}$ is a highly conserved aromatic residue in GPCRs (conserved at 97% in class A GPCRs[50]) located one helix turn from F237$^{4.46}$ and is also a contact residue for ORG27569[17] and cholesterol.[19] In our trajectories, W241$^{4.50}$ could form stacking or T-shape aromatic interactions with F237$^{4.46}$ in its "displaced" conformation (Figures S9 and S10), and such interactions would be lost in the F237L mutant CB1. Though contacts between F237$^{4.46}$ and W241$^{4.50}$ are observed in crystal structures of the receptor coupled to the G protein,[25,26] suggesting aromatic interactions between F237$^{4.46}$ and W241$^{4.50}$ are characteristic of the active state, the disruption of such interactions is likely not the only factor involved in the effect of F237L mutation upon activation. Actually, one of the important results in this study is the global effect of the mutation. While the perturbation of local aromatic interactions is probably relevant, we observed that the effects are nonlocal and widespread, affecting pairwise residue distances and contacts across CB1 structure. The dynamical coupling between the local network of aromatic residues and the global state of the receptor deserves further investigation. F155$^{2.42}$, F237$^{4.46}$, and W241$^{4.50}$ may work as an "allosteric micro-switch" that could be modulated by mutations, allosteric ligands, or membrane lipids. We believe this hypothesis should be further explored through new simulations with mutations of these residues, and also through metadynamics simulations, to probe free energy barriers associated to their conformational changes.

Experimental results showed that F237L increases CP55940 binding and reduces inverse agonist SR141716A binding.[17] Our simulations indicated that the F237L mutation had an impact on residues on the CP55940 binding site, and therefore they are consistent with the experimental verification that perturbations in F237$^{4.46}$ can affect orthosteric ligand binding. However, we have not been able to capture significant differences between *wt* and mutant affinities for CP55940. This can be explained by the relatively low difference in the experimentally determined CP55940 affinity between *wt* and F237L CB1 (K_d in *wt* CB1:8.7 ± 0.7 nM; K_d F237L CB1:5.0 ± 0.2 nM; data from Shao et al.[17]) and also by limitations in MMPBSA methodology, such as considering an implicit solvent and membrane. Also, the entropic component was not considered, which might be an important factor contributing to the free energy of binding, or perhaps altered by F237L mutation. Despite these limitations and inaccuracies introduced by docking, our results suggest that multiple residues in the CP55940 binding site are affected by F237L mutation, as shown by contact analysis and MMPBSA free energy decomposition (Figure 5). These results indicate a complex effect, with some protein−ligand interactions being more probable in *wt* CB1 and others favored in the mutant. Among the residues that display different contact frequencies with the agonist, I267^{ECL2}, P269^{ECL2}, and D272^{ECL2} are located in the ECL2; notably, contacts between the agonist and I267^{ECL2} and P269^{ECL2} are favored in the mutant. This is an interesting result, since it has been shown that ECL2 is a critical region for CP55940 binding.[46] One hypothesis is that the F237L mutation, by favoring these contacts, leads to a stronger interaction with ECL2 and facilitate agonist binding into a higher affinity state. The small difference in experimental affinities for CP55940 between *wt* and F237L CB1 poses a challenge to the corroboration of this hypothesis through simulations. Nevertheless, it could be interesting to use more sophisticated free energy estimation methods (e.g., funnel metadynamics[57]) to interrogate more closely the role of these ECL2 residues in the process of agonist binding. Mutations at these ECL2 sites could be tested both theoretically and experimentally to test the validity of our observations.

https://doi.org/10.1021/acsomega.2c04980
ACS Omega 2022, 7, 37873−37884

The F237L mutation exhibits a qualitatively similar effect to allosteric ligand binding. Mutations whose effect is similar to allosteric ligand binding have been reported before for other GPCRs. For example, in the metabotropic glutamate receptor 2 (mGluR2), it has been observed that Q679V and C770A mutations converted a partial agonist into a full agonist, therefore acting in a similar way as a positive allosteric modulator (PAM).[58] ORG27569 is one of the most studied CB1 allosteric modulators and has intriguing pharmacological properties in that it displays positive binding cooperativity and negative functional cooperativity with CB1 agonists such as CP55940. Allosteric modulators with this behavior have been previously denominated PAM-antagonists.[18] However, the mechanism by which ORG27569 exerts this effect is still unknown. In the CP55940 and ORG27569-bound crystal structure of CB1,[17] ORG27569 can be observed bound to the intracellular side of the receptor, in an extrahelical binding site formed by TM2 and TM4 that partially overlaps with a cholesterol binding site.[17,19] $F237^{4.46}$ is a contact residue for both ORG27569 and cholesterol binding as shown in these crystal structures. Moreover, F237L mutation causes an increase in the affinity of CP55940 for CB1[17] and, as examined in this study, impairs receptor activation. Furthermore, it has been shown that ORG27569 promotes receptor internalization,[20,59] an effect that is also observed in homologous F238L mutation in rat CB1.[60] When considered together, all these data and the shared effects between ORG27569 binding and F237L mutation, combined with the fact that $F237^{4.46}$ is a contact residue for ORG27569, suggest that $F237^{4.46}$ contributes to mediate its allosteric effects.

This study was limited to the analysis of F237L mutation. Since this mutation has a global effect on the receptor conformational properties, this indicates that this region is a potential hotspot for allosteric modulation in CB1. It would be expected that other perturbations in this region such as those resulting from ligand binding would affect distant regions of the receptor, thus suggesting a chemical space where a variety of allosteric ligands may be developed. Finally, we conclude that MD simulations on mutant receptor models, despite their inherent limitations and taken with the necessary caution,[61] can be used as an exploratory tool to provide clues for subsequent structure-based drug design of allosteric compounds.

■ ASSOCIATED CONTENT

Data Availability Statement

Atomic coordinates for the initial MD systems for *wt* and F237L CB1, both apo and bound to CP55940, as well as input files for MD simulations with ACEMD and MMPBSA calculations are provided in the Supporting Information. The following software was used: CHARMM-GUI (https://www.charmm-gui.org/), ACEMD2 (https://www.acellera.com/acemd/), MODELER 9.14 (https://salilab.org/modeller/), AUTODOCK 4.2 (https://autodock.scripps.edu/), CHIMERA 1.14 (https://www.cgl.ucsf.edu/chimera/), VMD 1.9.4 (https://www.ks.uiuc.edu/Research/vmd/), Bio3D 2.4.1 (http://thegrantlab.org/bio3d/), gmx_MMPBSA 1.4.3 (https://pypi.org/project/gmx-MMPBSA/) and GROMACS2020.4 (https://www.gromacs.org/). Graphs were generated with Matplotlib 2.2.5 (https://matplotlib.org/).

Supporting Information

The Supporting Information is available free of charge at https://pubs.acs.org/doi/10.1021/acsomega.2c04980.

Statistically significant differences in average pairwise residue distance between MD simulations of *wt* and F237L CB1 bound to CP55940 (ODS), protein and CP55940 RMSD over time for each replica, RMSF of all residues for each replica, structural comparison of docked CP55940 to cocrystallized CP55940, distance between CP55940 and $P269^{ECL2}$, CP55940 and $M384^{7.40}$, and $P151^{2.38}$ and $D338^{6.30}$ in MD simulations of *wt* and F237L CB1 bound to CP55940, differences in occupancy of water molecules for each residue in MD simulations of *wt* and F237L CB1 bound to CP55940, distances between residues $F155^{2.42}$, $F237^{4.46}$, and $W241^{4.50}$ and their configurations during MD simulations, contact frequencies of CP55940 with the receptor in MD simulations of *wt* and F237L CB1, *p*-values of performed statistical tests for the difference in CP55940 binding residue energy decomposition between *wt* and F237L CB1 (PDF)

Atomic coordinates for all models and input files for MD simulations and MMPBSA calculations (ZIP)

Differences in average residue pairwise distances between agonist-bound *wt* and agonist-bound mutant receptor (TXT)

■ AUTHOR INFORMATION

Corresponding Authors

Jesús Giraldo − *Laboratory of Molecular Neuropharmacology and Bioinformatics, Unitat de Bioestadística and Institut de Neurociències and Unitat de Neurociència Traslacional, Parc Taulí Hospital Universitari, Institut d'Investigació i Innovació Parc Taulí (I3PT), Institut de Neurociències, Universitat Autònoma de Barcelona, Bellaterra 08193, Spain; Instituto de Salud Carlos III, Centro de Investigación Biomédica en Red de Salud Mental (CIBERSAM), Madrid 28029, Spain;* orcid.org/0000-0001-7082-4695; Email: Jesus.Giraldo@uab.es

Pedro Renault − *Laboratory of Molecular Neuropharmacology and Bioinformatics, Unitat de Bioestadística and Institut de Neurociències and Unitat de Neurociència Traslacional, Parc Taulí Hospital Universitari, Institut d'Investigació i Innovació Parc Taulí (I3PT), Institut de Neurociències, Universitat Autònoma de Barcelona, Bellaterra 08193, Spain; Instituto de Salud Carlos III, Centro de Investigación Biomédica en Red de Salud Mental (CIBERSAM), Madrid 28029, Spain;* orcid.org/0000-0002-5649-3057; Email: Pedro.Renault@uab.cat

Author

Oscar Díaz − *Laboratory of Molecular Neuropharmacology and Bioinformatics, Unitat de Bioestadística and Institut de Neurociències and Unitat de Neurociència Traslacional, Parc Taulí Hospital Universitari, Institut d'Investigació i Innovació Parc Taulí (I3PT), Institut de Neurociències, Universitat Autònoma de Barcelona, Bellaterra 08193, Spain; Instituto de Salud Carlos III, Centro de Investigación Biomédica en Red de Salud Mental (CIBERSAM), Madrid 28029, Spain*

Complete contact information is available at: https://pubs.acs.org/10.1021/acsomega.2c04980

Author Contributions

MD simulations were performed and analyzed by Ó.D. P.R. and J.G. designed and supervised the study. The manuscript

https://doi.org/10.1021/acsomega.2c04980
ACS Omega 2022, 7, 37873−37884

was written through contributions of all authors. All authors have given approval to the final version of the manuscript.

Notes

The authors declare no competing financial interest.

■ ACKNOWLEDGMENTS

This project has received funding from the European Union's Horizon2020 research and innovation programme under grant agreement 848068 and from Ministerio de Ciencia e Innovación (Spain) under grant agreement PID2020-119136RB-I00. This publication reflects only the authors' view and the European Commission is not responsible for any use that may be made of the information it contains. We thank Xin Yang for providing the MD-generated receptor structures[23] at the end of this project.

■ ABBREVIATIONS

CB1, cannabinoid receptor 1; GPCR, G protein-coupled receptor; THC, Δ9-tetrahydrocannabinol; TM, transmembrane helix; ICL, intracellular loop; ECL, extracellular loop; PDB, Protein Data Bank; NAM, negative allosteric modulator; PAM, positive allosteric modulator; POPC, 1-palmitoyl-2-oleoyl-sn-glycero-3-phosphocoline; MMPBSA, molecular mechanics Poisson−Boltzmann surface area

■ REFERENCES

(1) Marsicano, G.; Lutz, B. Expression of the Cannabinoid Receptor CB1 in Distinct Neuronal Subpopulations in the Adult Mouse Forebrain. *Eur. J. Neurosci.* **1999**, *11* (12), 4213−4225.
(2) Reggio, P. H. Endocannabinoid Binding to the Cannabinoid Receptors: What Is Known and What Remains Unknown. *Curr. Med. Chem.* **2010**, *17* (14), 1468−1486.
(3) Mechoulam, R.; Parker, L. A. The Endocannabinoid System and the Brain. *Annu. Rev. Psychol.* **2013**, *64*, 21−47.
(4) Pertwee, R. Pharmacological Actions of Cannabinoids. In *Cannabinoids*; Pertwee, R., Ed.; Springer, 2005; pp 1−51.
(5) Janero, D. R.; Makriyannis, A. Cannabinoid Receptor Antagonists: Pharmacological Opportunities, Clinical Experience, and Translational Prognosis. *Expert Opin. Emerg. Drugs* **2009**, *14* (1), 43−65.
(6) Lipnik-Štangelj, M.; Razinger, B. A Regulatory Take on Cannabis and Cannabinoids for Medicinal Use in the European Union. *Arh. Hig. Rada Toksikol.* **2020**, *71* (1), 12−18.
(7) Giraldo, J. How Inverse Can a Neutral Antagonist Be? Strategic Questions after the Rimonabant Issue. *Drug Discovery Today* **2010**, *15* (11−12), 411−415.
(8) Melancon, B. J.; Hopkins, C. R.; Wood, M. R.; Emmitte, K. A.; Niswender, C. M.; Christopoulos, A.; Conn, P. J.; Lindsley, C. W. Allosteric Modulation of Seven Transmembrane Spanning Receptors: Theory, Practice, and Opportunities for Central Nervous System Drug Discovery. *J. Med. Chem.* **2012**, *55* (4), 1445−1464.
(9) Fasciani, I.; Petragnano, F.; Aloisi, G.; Marampon, F.; Carli, M.; Scarselli, M.; Maggio, R.; Rossi, M. Allosteric Modulators of g Protein-Coupled Dopamine and Serotonin Receptors: A New Class of Atypical Antipsychotics. *Pharmaceuticals* **2020**, *13* (11), 388.
(10) Christopoulos, A.; Kenakin, T. G Protein-Coupled Receptor Allosterism and Complexing. *Pharmacol. Rev.* **2002**, *54* (2), 323−374.
(11) Foster, D. J.; Conn, P. J. Allosteric Modlation of GPCRs: New Insights and Potential Utility for Treatment of Schizophrenia and Other CNS Disorders. *Neuron* **2017**, *94* (3), 431−446.
(12) Price, M. R.; Baillie, G. L.; Thomas, A.; Stevenson, L. a; Easson, M.; Goodwin, R.; Mclean, A.; Mcintosh, L.; Goodwin, G.; Walker, G.; Westwood, P.; Marrs, J.; Thomson, F.; Cowley, P.; Christopoulos, A.; Pertwee, R. G.; Ross, R. A. Allosteric Modulation of the Cannabinoid CB1 Receptor. *Mol. Pharmacol.* **2005**, *68* (5), 1484−1495.
(13) Horswill, J. G.; Bali, U.; Shaaban, S.; Keily, J. F.; Jeevaratnam, P.; Babbs, A. J.; Reynet, C.; Wong Kai In, P. PSNCBAM-1, a Novel Allosteric Antagonist at Cannabinoid CB 1 Receptors with Hypophagic Effects in Rats. *Br. J. Pharmacol.* **2007**, *152* (5), 805−814.
(14) Immadi, S. S.; Dopart, R.; Wu, Z.; Fu, B.; Kendall, D. A.; Lu, D. Exploring 6-Azaindole and 7-Azaindole Rings for Developing Cannabinoid Receptor 1 Allosteric Modulators. *Cannabis Cannabinoid Res.* **2018**, *3* (1), 252−258.
(15) Laprairie, R. B.; Kulkarni, P. M.; Deschamps, J. R.; Kelly, M. E. M.; Janero, D. R.; Cascio, M. G.; Stevenson, L. A.; Pertwee, R. G.; Kenakin, T. P.; Denovan-Wright, E. M.; Thakur, G. A. Enantiospecific Allosteric Modulation of Cannabinoid 1 Receptor. *ACS Chem. Neurosci.* **2017**, *8* (6), 1188−1203.
(16) Nguyen, T.; Li, J.-X.; Thomas, B. F.; Wiley, J. L.; Kenakin, T. P.; Zhang, Y. Allosteric Modulation: An Alternate Approach Targeting the Cannabinoid CB1 Receptor. *Med. Res. Rev.* **2017**, *37* (3), 441−474.
(17) Shao, Z.; Yan, W.; Chapman, K.; Ramesh, K.; Ferrell, A. J.; Yin, J.; Wang, X.; Xu, Q.; Rosenbaum, D. M. Structure of an Allosteric Modulator Bound to the CB1 Cannabinoid Receptor. *Nat. Chem. Biol.* **2019**, *15*, 1199−1205.
(18) Kenakin, T.; Strachan, R. T. PAM-Antagonists: A Better Way to Block Pathological Receptor Signaling? *Trends Pharmacol. Sci.* **2018**, *39* (8), 748−765.
(19) Hua, T.; Vemuri, K.; Nikas, S. P.; Laprairie, R. B.; Wu, Y.; Qu, L.; Pu, M.; Korde, A.; Jiang, S.; Ho, J.-H.; Han, G. W.; Ding, K.; Li, X.; Liu, H.; Hanson, M. A.; Zhao, S.; Bohn, L. M.; Makriyannis, A.; Stevens, R. C.; Liu, Z.-J. Crystal Structures of Agonist-Bound Human Cannabinoid Receptor CB1. *Nature* **2017**, *547* (7664), 468−471.
(20) Stornaiuolo, M.; Bruno, A.; Botta, L.; Regina, G. La; Cosconati, S.; Silvestri, R.; Marinelli, L.; Novellino, E. Endogenous vs Exogenous Allosteric Modulators in GPCRs: A Dispute for Shuttling CB1 among Different Membrane Microenvironments. *Sci. Rep.* **2015**, *5* (1), 1−13.
(21) Bari, M.; Paradisi, A.; Pasquariello, N.; Maccarrone, M. Cholesterol-Dependent Modulation of Type 1 Cannabinoid Receptors in Nerve Cells. *J. Neurosci. Res.* **2005**, *81* (2), 275−283.
(22) Ballesteros, J. A.; Weinstein, H. Integrated Methods for the Construction of Three-Dimensional Models and Computational Probing of Structure-Function Relations in G Protein-Coupled Receptors. *Methods Neurosci.* **1995**, *25*, 366−428.
(23) Yang, X.; Wang, X.; Xu, Z.; Wu, C.; Zhou, Y.; Wang, Y.; Lin, G.; Li, K.; Wu, M.; Xia, A. Molecular Mechanism of Allosteric Modulation for the Cannabinoid Receptor CB1. *Nat. Chem. Biol.* **2022**, *18*, 831.
(24) Shao, Z.; Yin, J.; Chapman, K.; Grzemska, M.; Clark, L.; Wang, J.; Rosenbaum, D. M. High-Resolution Crystal Structure of the Human CB1 Cannabinoid Receptor. *Nature* **2016**, *540* (7634), 602−606.
(25) Krishna Kumar, K.; Shalev-Benami, M.; Robertson, M. J.; Hu, H.; Banister, S. D.; Hollingsworth, S. A.; Latorraca, N. R.; Kato, H. E.; Hilger, D.; Maeda, S.; Weis, W. I.; Farrens, D. L.; Dror, R. O.; Malhotra, S. V.; Kobilka, B. K.; Skiniotis, G. Structure of a Signaling Cannabinoid Receptor 1-G Protein Complex. *Cell* **2019**, *176* (3), 448−458 e12.
(26) Hua, T.; Li, X.; Wu, L.; Iliopoulos-Tsoutsouvas, C.; Wang, Y.; Wu, M.; Shen, L.; Brust, C. A.; Nikas, S. P.; Song, F.; Song, X.; Yuan, S.; Sun, Q.; Wu, Y.; Jiang, S.; Grim, T. W.; Benchama, O.; Stahl, E. L.; Zvonok, N.; Zhao, S.; Bohn, L. M.; Makriyannis, A.; Liu, Z. J. Activation and Signaling Mechanism Revealed by Cannabinoid Receptor-Gi Complex Structures. *Cell* **2020**, *180* (4), 655−665.
(27) Díaz, Ó.; Dalton, J. A. R.; Giraldo, J. Revealing the Mechanism of Agonist-Mediated Cannabinoid Receptor 1 (CB1) Activation and Phospholipid-Mediated Allosteric Modulation. *J. Med. Chem.* **2019**, *62* (11), 5638−5654.
(28) Webb, B.; Sali, A. Comparative Protein Structure Modeling Using MODELLER. *Curr. Protoc. Bioinforma.* **2014**, *47*, 5.6.1−5.6.32.
(29) Morris, G. M.; Huey, R.; Lindstrom, W.; Sanner, M. F.; Belew, R. K.; Goodsell, D. S.; Olson, A. J. AutoDock4 and AutoDockTools4:

https://doi.org/10.1021/acsomega.2c04980
ACS Omega 2022, 7, 37873−37884

Automated Docking with Selective Receptor Flexibility. *J. Comput. Chem.* **2009**, *30* (16), 2785−2791.
(30) Pettersen, E. F.; Goddard, T. D.; Huang, C. C.; Couch, G. S.; Greenblatt, D. M.; Meng, E. C.; Ferrin, T. E. UCSF Chimera—A Visualization System for Exploratory Research and Analysis. *J. Comput. Chem.* **2004**, *25* (13), 1605−1612.
(31) Shapovalov, M. V.; Dunbrack, R. L. A Smoothed Backbone-Dependent Rotamer Library for Proteins Derived from Adaptive Kernel Density Estimates and Regressions. *Structure* **2011**, *19* (6), 844−858.
(32) Lans, I.; Dalton, J. A. R.; Giraldo, J. Selective Protonation of Acidic Residues Triggers Opsin Activation. *J. Phys. Chem. B* **2015**, *119* (30), 9510−9519.
(33) Bruzzese, A.; Gil, C.; Dalton, J. A. R.; Giraldo, J. Structural Insights into Positive and Negative Allosteric Regulation of a G Protein-Coupled Receptor through Protein-Lipid Interactions. *Sci. Rep.* **2018**, *8* (1), 4456.
(34) Bruzzese, A.; Dalton, J. A. R.; Giraldo, J. Insights into Adenosine A2A Receptor Activation through Cooperative Modulation of Agonist and Allosteric Lipid Interactions. *PLoS Computat. Biol.* **2020**, *16*, e1007818.
(35) Harvey, M. J.; Giupponi, G.; De Fabritiis, G. ACEMD: Accelerating Biomolecular Dynamics in the Microsecond Time Scale. *J. Chem. Theory Comput.* **2009**, *5* (6), 1632−1639.
(36) Huang, J.; MacKerell, A. D. CHARMM36 All-Atom Additive Protein Force Field: Validation Based on Comparison to NMR Data. *J. Comput. Chem.* **2013**, *34* (25), 2135−2145.
(37) Vanommeslaeghe, K.; Hatcher, E.; Acharya, C.; Kundu, S.; Zhong, S.; Shim, J.; Darian, E.; Guvench, O.; Lopes, P.; Vorobyov, I.; MacKerell Jr, A. D. CHARMM General Force Field (CGenFF): A Force Field for Drug-like Molecules Compatible with the CHARMM All-Atom Additive Biological Force Fields. *J. Comput. Chem.* **2010**, *31* (4), 671−690.
(38) Vanommeslaeghe, K.; MacKerell, A. D. J. Automation of the CHARMM General Force Field (CGenFF) I: Bond Perception and Atom Typing. *J. Chem. Inf. Model.* **2012**, *52* (12), 3144−3154.
(39) Humphrey, W.; Dalke, A.; Schulten, K. VMD: Visual Molecular Dynamics. *J. Mol. Graph.* **1996**, *14* (1), 33−38.
(40) Lindahl, E.; Hess, B.; van der Spoel, D. GROMACS 3.0: A Package for Molecular Simulation and Trajectory Analysis. *Mol. Model. Annu.* **2001**, *7* (8), 306−317.
(41) Grant, B. J.; Rodrigues, A. P. C.; ElSawy, K. M.; McCammon, J. A.; Caves, L. S. D. Bio3d: An R Package for the Comparative Analysis of Protein Structures. *Bioinformatics* **2006**, *22* (21), 2695−2696.
(42) Miller, B. R.; McGee, T. D.; Swails, J. M.; Homeyer, N.; Gohlke, H.; Roitberg, A. E. MMPBSA.py: An E Ffi Cient Program for End-State Free Energy Calculations. *J. Chem. Theory Comput.* **2012**, *8*, 3314−3321.
(43) Katritch, V.; Cherezov, V.; Stevens, R. C. Structure-Function of the G-Protein-Coupled Receptor Superfamily. *Annu. Rev. Pharmacol. Toxicol.* **2013**, *53*, 531−556.
(44) Hua, T.; Vemuri, K.; Pu, M.; Qu, L.; Han, G. W.; Wu, Y.; Zhao, S.; Shui, W.; Li, S.; Korde, A.; Laprairie, R. B.; Stahl, E. L.; Ho, J. H.; Zvonok, N.; Zhou, H.; Kufareva, I.; Wu, B.; Zhao, Q.; Hanson, M. A.; Bohn, L. M.; Makriyannis, A.; Stevens, R. C.; Liu, Z. J. Crystal Structure of the Human Cannabinoid Receptor CB1. *Cell* **2016**, *167* (3), 750−762.
(45) McAllister, S. D.; Hurst, D. P.; Barnett-Norris, J.; Lynch, D.; Reggio, P. H.; Abood, M. E. Structural Mimicry in Class A G Protein-Coupled Receptor Rotamer Toggle Switches: The Importance of the F3.36(201)/W6.48(357) Interaction in Cannabinoid CB1 Receptor Activation. *J. Biol. Chem.* **2004**, *279* (46), 48024−48037.
(46) Ahn, K. H.; Bertalovitz, A. C.; Mierke, D. F.; Kendall, D. A. Dual Role of the Second Extracellular Loop of the Cannabinoid Receptor 1 : Ligand Binding and Receptor Localization. *Mol. Pharmacol.* **2009**, *76* (4), 833−842.
(47) Shim, J. Y.; Bertalovitz, A. C.; Kendall, D. A. Identification of Essential Cannabinoid-Binding Domains: Structural Insights into Early Dynamic Events in Receptor Activation. *J. Biol. Chem.* **2011**, *286* (38), 33422−33435.
(48) Kapur, A.; Hurst, D. P.; Fleischer, D.; Whitnell, R.; Thakur, G. A.; Makriyannis, A.; Reggio, P. H.; Abood, M. E. Mutation Studies on Ser7.39 and Ser2.60 in the Human CB1 Receptor: Evidence for a Serine-Induced Bend in CB1 Transmembrane Helix 7. *Mol. Pharmacol.* **2007**, *71* (6), 1512−1524.
(49) Dalton, J. A. R.; Lans, I.; Giraldo, J. Quantifying Conformational Changes in GPCRs: Glimpse of a Common Functional Mechanism. *BMC Bioinformatics* **2015**, *16*, 124.
(50) Isberg, V.; de Graaf, C.; Bortolato, A.; Cherezov, V.; Katritch, V.; Marshall, F. H.; Mordalski, S.; Pin, J.-P.; Stevens, R. C.; Vriend, G.; Gloriam, D. E. Generic GPCR Residue Numbers - Aligning Topology Maps While Minding the Gaps. *Trends Pharmacol. Sci.* **2015**, *36* (1), 22−31.
(51) Guixà-González, R.; Albasanz, J. L.; Rodriguez-Espigares, I.; Pastor, M.; Sanz, F.; Martí-Solano, M.; Manna, M.; Martinez-Seara, H.; Hildebrand, P. W.; Martín, M.; Selent, J. Membrane Cholesterol Access into a G-Protein-Coupled Receptor. *Nat. Commun.* **2017**, *8*, 14505.
(52) Oddi, S.; Dainese, E.; Fezza, F.; Lanuti, M.; Barcaroli, D.; De Laurenzi, V.; Centonze, D.; Maccarrone, M. Functional Characterization of Putative Cholesterol Binding Sequence (CRAC) in Human Type-1 Cannabinoid Receptor. *J. Neurochem.* **2011**, *116* (5), 858−865.
(53) Niesen, M. J. M.; Bhattacharya, S.; Vaidehi, N. The Role of Conformational Ensembles in Ligand Recognition in G-Protein Coupled Receptors. *J. Am. Chem. Soc.* **2011**, *133* (33), 13197−13204.
(54) Wang, X.; Liu, D.; Shen, L.; Li, F.; Li, Y.; Yang, L.; Xu, T.; Tao, H.; Yao, D.; Wu, L.; Hirata, K.; Bohn, L. M.; Makriyannis, A.; Liu, X.; Hua, T.; Liu, Z.; Wang, J. A Genetically Encoded F - 19 NMR Probe Reveals the Allosteric Modulation Mechanism of Cannabinoid Receptor 1. *J. Am. Chem. Soc.* **2021**, *143* (40), 16320−16325.
(55) Yuan, S.; Vogel, H.; Filipek, S. The Role of Water and Sodium Ions in the Activation of the μ-Opioid Receptor. *Angew. Chem., Int. Ed. Engl.* **2013**, *52* (38), 10112−10115.
(56) Yuan, S.; Hu, Z.; Filipek, S.; Vogel, H. W246(6.48) Opens a Gate for a Continuous Intrinsic Water Pathway during Activation of the Adenosine A2A Receptor. *Angew. Chem., Int. Ed. Engl.* **2015**, *54* (2), 556−559.
(57) Limongelli, V.; Bonomi, M.; Parrinello, M. Funnel Metadynamics as Accurate Binding Free-Energy Method. *Proc. Natl. Acad. Sci. U. S. A.* **2013**, *110* (16), 6358−6363.
(58) Doumazane, E.; Scholler, P.; Fabre, L.; Zwier, J. M.; Trinquet, E.; Pin, J. P.; Rondard, P. Illuminating the Activation Mechanisms and Allosteric Properties of Metabotropic Glutamate Receptors. *Proc. Natl. Acad. Sci. U. S. A.* **2013**, *110* (15), E1416.
(59) Ahn, K. H.; Mahmoud, M. M.; Kendall, D. A. Allosteric Modulator ORG27569 Induces CB1 Cannabinoid Receptor High Affinity Agonist Binding State, Receptor Internalization, and Gi Protein-Independent ERK1/2 Kinase Activation. *J. Biol. Chem.* **2012**, *287* (15), 12070−12082.
(60) Wickert, M.; Hildick, K. L.; Baillie, G. L.; Jelinek, R.; Aparisi Rey, A.; Monory, K.; Schneider, M.; Ross, R. A.; Henley, J. M.; Lutz, B. The F238L Point Mutation in the Cannabinoid Type 1 Receptor Enhances Basal Endocytosis via Lipid Rafts. *Front. Mol. Neurosci.* **2018**, *11* (July), 1−11.
(61) Giraldo, J. Agonist Induction, Conformational Selection, and Mutant Receptors. *FEBS Lett.* **2004**, *556* (1−3), 13−18.

https://doi.org/10.1021/acsomega.2c04980
ACS Omega 2022, 7, 37873−37884